Pergamon

Geochimica et Cosmochimica Acta, Vol. 68, No. 3, pp. 423–432, 2004

0016-7037/04 $30.00 + .00

doi:10.1016/S0016-7037(00)00453-8

Determination of Sr and Ba partition coefficients between apatite and water from 5°C to 60°C: A potential new thermometer for aquatic paleoenvironments

V. BALTER* and C. LÉCUYER†

UMR 5125 CNRS "PaléoEnvironnements and PaléobioSphère," Université Claude Bernard Lyon 1, Campus de la Doua, Bâtiment Géode, Boulevard du 11/11/1918, 69622 Villeurbanne Cedex, France

(*Received October* 8, 2002; *accepted in revised form June* 6, 2003)

Abstract—Apparent partition coefficients of Sr and Ba between calcium phosphate and water were measured experimentally for temperature ranging from 5°C to 60°C. Calcium phosphates were precipitated from an aqueous mixture of $Na_2HPO_4 \cdot 2H_2O$ (10^{-2} M) and $CaCl_2 \cdot 2H_2O$ (10^{-2} M). Spiked solutions of Sr or Ba were introduced into the $CaCl_2 \cdot 2H_2O$ solution at Sr/Ca and Ba/Ca ratios of 0.1. The experiment consisted in sampling the liquid and solid phases after 1, 6, 48, and 96 h of interaction. The amorphous calcium phosphate (ACP) precipitated early in the experiment was progressively replaced by hydroxylapatite (HAP), except at 5°C where brushite (di-calcium phosphate di-hydrate or DCPD) was formed. We observed that the crystallinity of the solid phase increased with time for a given temperature and increased with temperature for a given time of reaction. With the exception of the experiment at 5°C, yield (R%) and apparent partition coefficients ($K_{a\text{-}w}^{Sr/Ca}$ and $K_{a\text{-}w}^{Ba/Ca}$) both decreased with increasing reaction time. After 96 h, R%, $K_{a\text{-}w}^{Sr/Ca}$ and $K_{a\text{-}w}^{Ba/Ca}$ were observed to be constant, suggesting that the solid phases were at steady-state with respect to the aqueous solutions. The thermodependence of Sr and Ba partitioning between apatite and water at low temperature could therefore be calculated:

$$\mathrm{Log}(K_{a\text{-}w}^{Sr/Ca}) = 0.42 \pm 0.04\,(10^3 T^{-1}) - 1.87 \pm 0.12\ (r^2 = 0.94)$$

$$\mathrm{Log}(K_{a\text{-}w}^{Ba/Ca}) = 1.96 \pm 0.06\,(10^3 T^{-1}) - 7.19 \pm 0.20\ (r^2 = 0.99)$$

We also performed competition experiments between Sr and Ba. The thermodependence of the Sr/Ba partitioning between apatite and water was calculated after 96 h of reaction:

$$\mathrm{Log}(K_{a\text{-}w}^{Sr/Ba}) = -0.75 \pm 0.04\,(10^3 T^{-1}) + 2.39 \pm 0.14\ (r^2 = 0.97)$$

This relationship reveals a discrimination of Ba in favor of Sr during their incorporation into HAP. Temperature trends deduced from the Ba/Ca of fish teeth recovered from the K/T boundary mimic those estimated from $\delta^{18}O(PO_4)$ measurements carried out on the same sample. Unless Sr, Ba and Ca contents of biogenic apatites are modified during diagenesis, their elemental ratios could be used as new and attractive thermometers of aquatic paleoenvironments.

1. INTRODUCTION

The thermodependence of the oxygen isotope fractionation between phosphate and water has been extensively used to reconstruct paleotemperatures in the aquatic environment (e.g., Longinelli and Nuti, 1973; Kolodny et al., 1983). The determination of paleotemperatures requires the measurement of the oxygen isotope composition of the water ($\delta^{18}O_w$) from which the phosphate precipitates. For example, in marine environments, the oxygen isotope ratio of seawater is sensitive to the local (evaporation versus precipitation) or global (development of ice caps) water budget. Variations of about ± 2‰ around the SMOW value are common in surficial marine waters from low to high latitudes (Pucéat et al., 2003). An uncertainty of 1‰ in the composition of the ambient water corresponds to an uncertainty of 4°C in the calculated paleotemperature using $\delta^{18}O_{PO4,}$ which is of the same order of magnitude than the short-term (10^4 yr) and long-term (10^7 yr) climatic fluctuations (Pucéat et al., 2003, Lécuyer et al., 2003)

Similar thermodependences of the oxygen isotope fractionation between PO_4-H_2O and CO_3-H_2O preclude the use of the ΔCO_3-PO_4 oxygen fractionation as a paleothermometer (Wenzel et al., 2000). Indirect determinations of the oxygen isotope composition of ambient waters are possible when combining $\delta^{18}O$ measurements of PO_4 from coeval ectotherm and homeotherm organisms (Kolodny et al., 1983; Lécuyer et al., 1996). However, such faunal assemblages remain relatively scarce in the fossil record and are mostly restricted to the post-Mesozoic.

The Ba concentrations in the oceans are not constant and are positively correlated to those of silica and alkalinity (Paytan and Kastner, 1996). However, at a global scale, the Ba concentrations in seawater seems to be regulated by an equilibrium with solid barium sulfate (Monnin et al., 1999). Since the Sr/Ca ratio is insensitive to changes in water salinity, it can be used to solve both temperature and salinity variables when combined to oxygen isotope ratios. Such a method, for example, has been successfully applied to carbonates, and more specifically to corals to identify flooding, upwelling or monsoon events (e.g., McCulloch et al., 1994). By analogy, Sr/Ca and Ba/Ca ratios of

* Author to whom correspondence should be addressed (Vincent.Balter@univ-lyon1.fr).
†*Present address:* Institut Universitaire de France, 103 Bd Saint Michel, 75005 Paris, France.

Table 1. Ca, Sr and Ba concentrations of the blanks and phosphate International Standards.

Blanks	Number of replicates	Ca (μg/L) Mean	Ca (μg/L) S.D.	Sr (μg/L) Mean	Sr (μg/L) S.D.	Ba (μg/L) Mean	Ba (μg/L) S.D.
$Na_2HPO_4 \cdot 2H_2O$	2	bdl	bdl	28.5	0.5	bdl	bdl
$CaCl_2 \cdot 2H_2O$	2	–	–	249	2	2.8	1.3
H_2O_{DD}	5	bdl	bdl	0.1	0.1	0.6	0.6

Standards	Number of replicates	Ca (mg/g) Mean	Ca (mg/g) S.D.	Sr (μg/g) Mean	Sr (μg/g) S.D.	Ba (μg/g) Mean	Ba (μg/g) S.D.
NBS120C	16	346	11	1008	43	76	1
Certified value		343	1	845§		–	
BCR32	12	367	10	972	49	105	1
Certified value		369	2	–		–	
SRM1400	3	405	9	252	2	245	3
Certified value		381	1	248	7	240§	

bdl: below detection limit; –: not applicable; §: reported but not a certified value.

well preserved biogenic apatites can be used as new proxies of aquatic paleotemperatures.

We experimentally determined the Sr and Ba partition coefficients between inorganic apatite and water at low temperatures (5°C to 60°C). The evolution of the crystal-chemical properties of the solid phase determining the $K_{a\text{-}w}^{Sr/Ca}$ and $K_{a\text{-}w}^{Ba/Ca}$ values as a function of time and temperature was also investigated. The thermodependence of $K_{a\text{-}w}^{Sr/Ca}$, $K_{a\text{-}w}^{Ba/Ca}$ and $K_{a\text{-}w}^{Sr/Ba}$ were calculated once steady-state conditions were reached. These results are compared with data available for living marine fish and applied to fish tooth enamels from the K/T boundary for which $\delta^{18}O(PO_4)$ values were previously determined (Lécuyer et al., 1993). Partitioning of Sr and Ba between biogenic apatite and water is a potential new paleothermometer although the effects of diagenesis and vital effects need to be evaluated before they are generally applied for paleoenvironmental reconstruction.

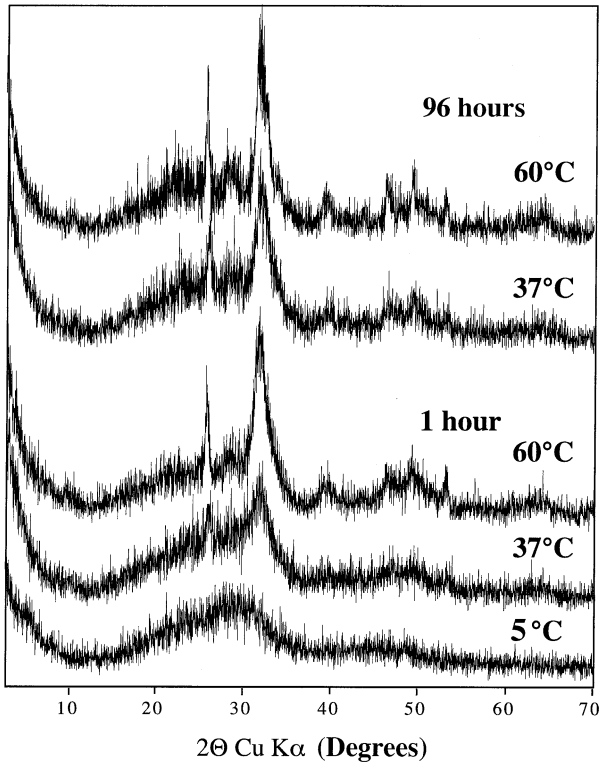

Fig. 1. Diffractograms of the PO_4^{3-}-bearing precipitates after 1 h and 96 h of maturation. The crystallinity increases with both time and temperature.

2. MATERIALS AND METHODS

2.1. Sr- and Ba-Enriched Precipitates

Various methods can promote the formation of Ca-bearing phosphates at low temperatures and wet conditions (e.g., Young and Holcomb, 1982; Van Cappellen and Berner, 1991). In this study, apatite was synthesized by mixing equal volumes of $Na_2HPO_4 \cdot 2H_2O$ (10^{-2} M) and $CaCl_2 \cdot 2H_2O$ (10^{-2} M), so that the concentrations of Ca and PO_4 are of the same order of magnitude as in blood plasma and seawater (except for P in seawater where the concentration is typically 2 μM: Broecker and Peng, 1982; Kaim and Schwederski, 1994). Sr or Ba enriched solutions (10,000 μg/mL) were added to the $CaCl_2 \cdot 2H_2O$ solution until a Sr/Ca or Ba/Ca ratio of 0.1 was reached. Because the experiments were not run at a constant ionic strength, we assumed that this initial ratio was high enough to avoid the total depletion of Sr and Ba in the solutions during the precipitation. All solutions were adjusted to a pH value of 10.8 by adding NaOH (10^{-1} M or 1 M). The resulting $Na_2HPO_4 \cdot 2H_2O$, $CaCl_2 \cdot 2H_2O$+Sr and $CaCl_2 \cdot 2H_2O$+Ba solutions had an ionic strength of 0.125 mol/L, 0.353 mol/L, and 1.171 mol/L respectively, comparable to blood plasma (0.3 mol/L) and seawater (0.7 mol/L). Some experiments were performed at a starting pH of 9.8 to evaluate the influence of the parent solution composition, on the chemistry of the solid phases. The solutions were filtered through a 0.22 μm filter and kept overnight at the desired temperature in sealed Erlenmeyer flasks. The temperature was controlled by a ThermoStat system and the experiments were carried out at 5, 25, 37, and 60°C. An additional set of experiments was carried out at 15°C for Ba. The Ca-bearing solution was rapidly poured into the P-containing solution, immediately initiating the nucleation of a solid phase. As a consequence of the nucleation and precipitation, the pH decreased from 10.8 to ~7.0. During the maturation of the solid phase, the Erlenmeyer flasks were gently shaken at regular intervals to avoid complete settling

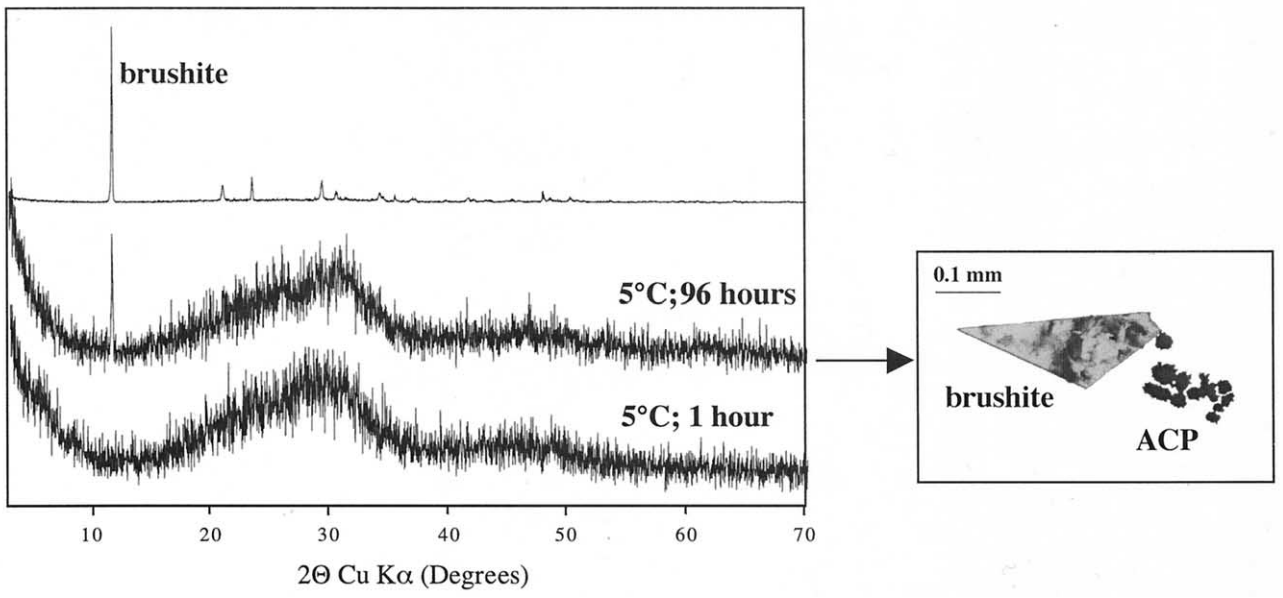

Fig. 2. Diffractograms and corresponding optical micrographs showing the coexistence of amorphous calcium phosphates (ACP) and brushite (dicalcium phosphate dihydrate, DCPD) (precipitated at 5°C after 96 h of maturation).

and the development of a concentration gradient in the solution. At the end of the experiment, the solid phase was separated from the supernatant by centrifugation, washed with distilled water and absolute ethanol and finally dried at room temperature. Triplicate experiments were systematically done.

We performed a second set of experiments to test the potential competition between Sr and Ba that substitute for Ca. A 1/1 (M) Sr and Ba mixture was added to the $CaCl_2 \cdot 2H_2O$ solution before mixing with the $Na_2HPO_4 \cdot 2H_2O$ solution. Adjusted to a pH of 10.8, these solutions had a ionic strength of 1.399 mol/L. The experiments were conducted for 96 h at 5, 25, 37 and 60°C.

2.2. Mineralogy and Trace Element Analysis

The mineralogy of the solid phase was determined by XRD (Cu Kα) using a D500 (Siemens) diffractometer. Sr, Ba, and Ca concentrations in the supernatant solution and associated solid phases were measured by ICP-AES and ICP-MS. In the latter case, indium was used as an internal standard and the masses ^{44}Ca, ^{88}Sr, and ^{137}Ba were used to avoid isobaric interference with Ar compounds. Distilled HNO_3 (4.5 mol/L) was used for the digestion of the solid phases. To check for possible Sr and Ba contamination in the starting material, blank measurements were done on the $CaCl_2 \cdot 2H_2O$ and $Na_2HPO_4 \cdot 2H_2O$ solutions (Table 1). Three international standards were used to assess the accuracy of the measurements: 1) the "Florida Phosphorite" SRM120c, 2) the "Bone Ash" SRM1400, both from the National Institute of Standards and Technology, and 3) the "Moroccan Phosphorite" BCR32 from the Institute for Reference Material and Measurements. We assumed that the partition coefficients for Sr and Ba between apatite and water, in relation to the design of the experiment, follow a homogeneous distribution law (McIntire, 1963) and were calculated according to the Henderson and Kracek (1927) equations:

$$K_{a\text{-}w}^{Sr/Ca} = (Sr/Ca)_{apatite}/(Sr/Ca)_{water} \text{ and}$$

$$K_{a\text{-}w}^{Ba/Ca} = (Ba/Ca)_{apatite}/(Ba/Ca)_{water} \quad (1)$$

The reaction yields (R%) were calculated on the basis of the total conversion of reactant in the solution into pure HAP with the stoichiometric formula $Ca_{10}(PO_4)_6(OH)_2$ (LeGeros and LeGeros, 1984).

3. RESULTS AND DISCUSSION

3.1. Evolution of the Precipitate Mineralogy

At a low supersaturation, the formation of crystallized HAP is achieved by the slow conversion of an unstable precursor ACP, which is constituted by a highly hydrated amorphous calcium phosphate (Eanes et al., 1965; Boskey and Posner, 1976; Nancollas, 1984; Abbona and Franchini-Angela, 1990). After 1 h of experiment, the solid phases were characterized by a poor crystallinity, as indicated by the width at half maximum (WHM) of the XRD peak, located around 32°, 2θ that is diagnostic of HAP (Fig. 1; JCPDS 1, 1990). The WHM could not be calculated at 5, 15, and 25°C as the diffraction patterns were too broad. Between 37 and 60°C, WHM decreased from 0.50 to 0.45. After 96 h of reaction, the crystallinity of the solid phase is higher with a WMH of 0.35 at 37°C and 0.30 at 60°C.

Whereas the crystallization of HAP at low supersaturation is systematically preceded by the formation of ACP, the mineralogical evolution of ACP may also lead to other phases such as brushite (DCPD: $CaHPO_4 0.2H_2O$) or octacalcium phosphate (OCP: $Ca_8H_2(PO_4)_6 0.5H_2O$) depending on the pH, Ca/P and temperature conditions at the beginning of the precipitation (Furedi-Milhofer et al., 1971; Brecevic and Furedi-Milhofer, 1972; Christoffersen et al., 1990). In our study, the XRD diffractograms of the 96-h precipitates match the diffraction pattern of HAP, meaning that the maturation of the precipitates promotes the conversion of ACP into HAP. This process is known to take place during the formation of bones, teeth, and sedimentary phosphates (e.g., Legeros and Legeros, 1984; Schenau et al., 2000). These results altogether reveal that the crystal-chemical properties of the synthesized HAP are time and temperature dependent.

At 5°C, there is no conversion of ACP into HAP. Instead, DCPD (JCPDS 2, 1990) appears after 96 h of maturation in

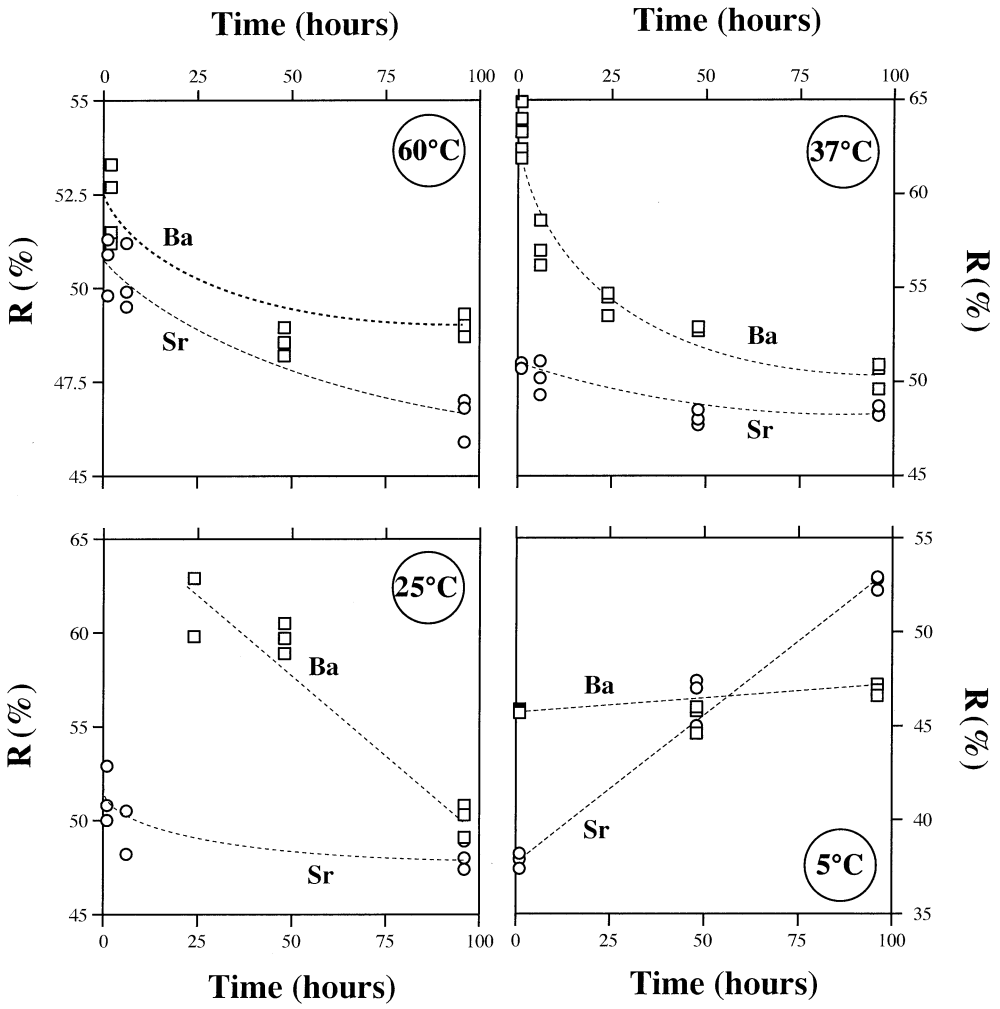

Fig. 3. Variations of the reaction yield (R%) with time for PO_4^{3-}-bearing precipitates at 5, 25, 37, and 60°C. Note the different scale for each temperature.

both the Sr and Ba-enriched starting solutions (Fig. 2). The mechanism of precipitation of DCPD during our experiments remains unclear. It could have been formed either by conversion of ACP or directly from the medium after the nucleation of ACP. Blake et al. (1998) precipitated calcium phosphate at 5°C from a phosphate source supplied by RNA, and did not observe the presence of DCPD upon SEM examination of the precipitate. Thus, the respective roles of seawater composition, temperature and the presence of an organic medium in the formation of sedimentary phosphates remain to be addressed.

3.2. Evolution of Yields

The reaction yields (R%) decrease with time at 25, 37 and 60°C but the trends are not systematic (Fig. 3). The change in yield with time is more important for Ba than for Sr, with almost a 10% decrease for Ba compared to 3% for Sr over the period of the experiments. In contrast, at 5°C, the reaction yields increase linearly with time for both the Sr and Ba-enriched precipitates. At 5°C, R% of the Sr-enriched precipitates increased by 15% whereas R% of the Ba-enriched precipitates varied by only 1% by the end of the experiment. The linear, positive evolution of the yields at 5°C may be explained by the constant rate of DCPD formation.

3.3. Evolution of Elemental Partitioning

From the results presented in Tables 2, 3, and 4, we can calculate that Sr and Ba are incorporated into the solid phases with mean concentrations of 0.54 and 0.44 mmol/g respectively. $K_{a\text{-}w}^{Sr/Ca}$ and $K_{a\text{-}w}^{Ba/Ca}$ decrease as a function of time at all temperatures and seem to reach steady-state values after ~96 h (Fig. 4). The $K_{a\text{-}w}^{Sr/Ca}$ and $K_{a\text{-}w}^{Ba/Ca}$ decreases are 10-fold greater at 5°C than at 25, 37 and 60°C. At these higher temperatures, the Sr, Ba, and Ca contents of the solid and liquid phases are consistent with a continuous incorporation of Ca into the solid phase and a simultaneous exclusion of Sr and Ba. The exclusion of Ba is more efficient than Sr, except at 60°C where they are similar. This may be explained by the ionic radii of Sr (1.33 Å) and Ba (1.5 Å) that are larger than Ca (1.08 Å). Thus, Ba, and to a lesser extent, Sr, which were easily incorporated into the poorly crystallized ACP nucleates, were partly

Table 2. Sr and Ca concentrations in the PO_4^{3-}-bearing liquid and solid phases, calculated Sr/Ca partition coefficients ($K_{a\text{-}w}^{Sr/Ca}$), and corresponding reaction yields (R%) of PO_4^{3-}-bearing precipitates. Each second line in italic indicates the respective standard deviation (SD) values.

Temperature (°C)	Time (hour)	Liquid phase			Solid phase				
		Sr (mmol/L)	Ca (mmol/L)	Sr/Ca	Sr (mmol/g)	Ca (mmol/g)	Sr/Ca	$K_{a\text{-}w}^{Sr/Ca}$	R (%)
60	96	0.34	1.45	0.233	0.49	8.86	0.055	0.237	46.6
		0.01	*0.08*	*0.006*	*0.01*	*0.03*	*0.001*	*0.006*	*0.5*
60	6	0.29	1.40	0.206	0.53	7.64	0.069	0.338	50.2
		0.01	*0.15*	*0.016*	*0.01*	*0.06*	*0.002*	*0.023*	*0.7*
60	1	0.26	1.15	0.225	0.54	7.26	0.075	0.332	50.8
		0.02	*0.19*	*0.018*	*0.01*	*0.16*	*0.003*	*0.011*	*2.9*
37	96	0.28	1.29	0.217	0.55	8.19	0.067	0.308	48.4
		0.01	*0.09*	*0.009*	*0.00*	*0.07*	*0.001*	*0.009*	*0.2*
37	48	0.28	1.41	0.200	0.56	8.20	0.069	0.349	48.1
		0.00	*0.14*	*0.020*	*0.01*	*0.08*	*0.001*	*0.042*	*0.3*
37	6	0.27	1.34	0.199	0.58	8.02	0.072	0.363	50.2
		0.00	*0.04*	*0.004*	*0.01*	*0.05*	*0.001*	*0.006*	*0.7*
37	1	0.27	1.42	0.190	0.54	7.68	0.070	0.371	50.8
		0.01	*0.06*	*0.004*	*0.01*	*0.15*	*0.000*	*0.009*	*0.1*
25	96	0.28	1.40	0.197	0.54	8.26	0.065	0.330	48.1
		0.00	*0.04*	*0.003*	*0.00*	*0.12*	*0.001*	*0.007*	*0.6*
25	6	0.27	1.59	0.173	0.54	7.69	0.070	0.410	48.9
		0.00	*0.12*	*0.013*	*0.01*	*0.07*	*0.002*	*0.043*	*1.6*
25	1	0.28	1.60	0.175	0.51	7.36	0.069	0.395	51.2
		0.01	*0.12*	*0.012*	*0.01*	*0.08*	*0.001*	*0.032*	*1.2*
5	96	0.27	1.60	0.170	0.52	7.32	0.070	0.416	52.6
		0.00	*0.07*	*0.005*	*0.01*	*0.13*	*0.000*	*0.012*	*0.3*
5	48	0.28	1.74	0.160	0.54	7.43	0.073	0.453	45.1
		0.00	*0.01*	*0.001*	*0.01*	*0.06*	*0.001*	*0.008*	*1.5*
5	1	0.29	2.09	0.138	0.54	6.53	0.083	0.601	37.8
		0.01	*0.10*	*0.003*	*0.01*	*0.07*	*0.001*	*0.006*	*0.4*

Table 3. Ba and Ca concentrations in the PO_4^{3-}-bearing liquid and solid phases, calculated Ba/Ca partition coefficients ($K_{a\text{-}w}^{Ba/Ca}$), and corresponding reaction yields (R%) of PO_4^{3-}-bearing precipitates. Each second line in italic indicates the respective SD values.

Temperature (°C)	Time (hour)	Liquid phase			Solid phase				
		Ba (mmol/L)	Ca (mmol/L)	Ba/Ca	Ba (mmol/g)	Ca (mmol/g)	Ba/Ca	$K_{a\text{-}w}^{Ba/Ca}$	R (%)
60	96	0.44	0.83	1.834	0.23	8.74	0.089	0.049	49.0
		0.00	*0.03*	*0.077*	*0.00*	*0.16*	*0.002*	*0.003*	*0.3*
60	48	0.43	1.09	1.363	0.18	8.17	0.077	0.057	47.3
		0.01	*0.05*	*0.057*	*0.01*	*0.06*	*0.003*	*0.002*	*0.7*
60	1	0.36	0.97	1.288	0.33	7.49	0.152	0.119	50.0
		0.01	*0.08*	*0.070*	*0.03*	*0.10*	*0.013*	*0.013*	*3.3*
37	96	0.36	1.06	1.198	0.35	7.66	0.156	0.133	50.4
		0.01	*0.16*	*0.181*	*0.01*	*0.04*	*0.004*	*0.017*	*0.6*
37	48	0.33	1.20	0.956	0.33	7.59	0.151	0.161	52.8
		0.01	*0.22*	*0.153*	*0.00*	*0.21*	*0.006*	*0.019*	*0.1*
37	24	0.29	1.33	0.755	0.37	7.26	0.175	0.235	54.2
		0.01	*0.15*	*0.073*	*0.01*	*0.14*	*0.005*	*0.031*	*0.5*
37	6	0.27	1.31	0.722	0.40	6.75	0.205	0.284	57.3
		0.00	*0.03*	*0.023*	*0.01*	*0.04*	*0.006*	*0.013*	*1.0*
37	1	0.25	1.33	0.631	0.44	6.60	0.228	0.361	63.1
		0.00	*0.04*	*0.024*	*0.03*	*0.45*	*0.004*	*0.010*	*1.6*
25	96	0.30	1.12	0.923	0.46	7.40	0.214	0.232	50.1
		0.01	*0.05*	*0.030*	*0.00*	*0.18*	*0.006*	*0.006*	*0.7*
25	48	0.23	1.46	0.553	0.48	6.20	0.268	0.487	59.7
		0.01	*0.03*	*0.037*	*0.01*	*0.07*	*0.006*	*0.040*	*0.7*
25	24	0.23	1.47	0.540	0.48	6.00	0.276	0.511	61.5
		0.00	*0.01*	*0.008*	*0.01*	*0.04*	*0.006*	*0.003*	*1.9*
15	96	0.28	1.58	0.175	0.26	3.64	0.071	0.405	71.7
		0.01	*0.05*	*0.007*	*0.01*	*0.18*	*0.001*	*0.018*	*6.3*
5	96	0.18	1.10	0.552	0.72	6.22	0.397	0.718	46.9
		0.00	*0.03*	*0.007*	*0.01*	*0.02*	*0.004*	*0.017*	*0.2*
5	48	0.08	1.08	0.249	0.61	6.56	0.318	1.280	41.5
		0.01	*0.04*	*0.016*	*0.02*	*0.24*	*0.011*	*0.066*	*2.5*
5	1	0.13	1.66	0.271	0.78	5.70	0.470	1.742	45.8
		0.01	*0.11*	*0.014*	*0.01*	*0.07*	*0.010*	*0.127*	*0.1*

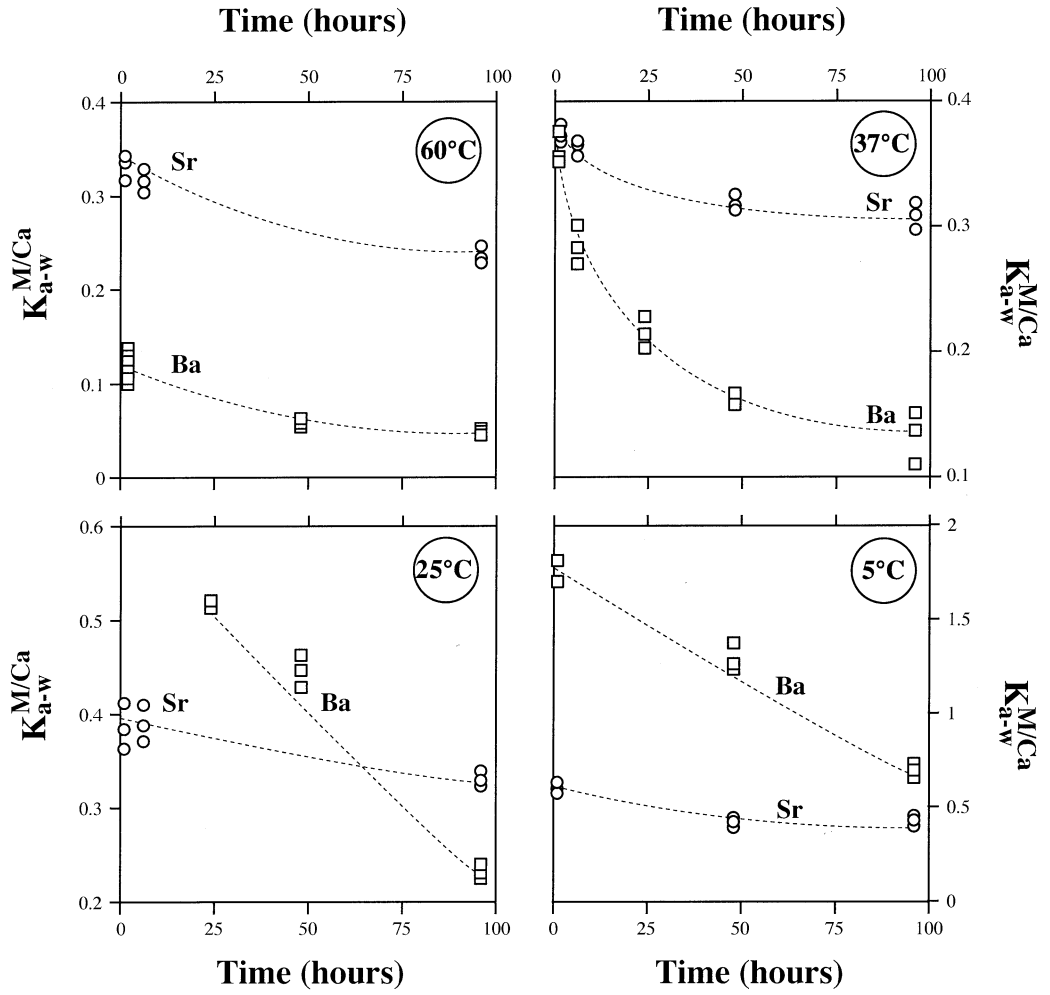

Fig. 4. Variations of the Sr and Ba partition coefficients ($K_{a\text{-}w}^{Sr/Ca}$ and $K_{a\text{-}w}^{Ba/Ca}$) with time for 5, 25, 37, and 60°C. The superscript "M" stands for the considered metal. Note the different scale for each temperature.

removed during the HAP maturation as a consequence of the restoration of the defects in the crystal lattice.

At 5°C, the interpretation of the results is difficult since the Sr, Ba, and Ca contents of the solid phase were measured on bulk samples, i.e., on a mixture of ACP and DCPD. The determination of the relative contributions of ACP and DCPD upon the evolution of $K_{a\text{-}w}^{Sr/Ca}$ and $K_{a\text{-}w}^{Ba/Ca}$ at 5°C by mass balance was not possible because in most cases DCPD and ACP were intimately mixed.

3.4. Intercorrelation between Yield and Partitioning

As a result of the time dependency of R%, $K_{a\text{-}w}^{Sr/Ca}$, and $K_{a\text{-}w}^{Ba/Ca}$, there is an intercorrelation between $K_{a\text{-}w}^{Sr/Ca}$, $K_{a\text{-}w}^{Ba/Ca}$, and R% for the experiments conducted at 25, 37, and 60°C with the slopes of the regression lines being similar at all temperatures, 36.9 (±4.5) and 46.6 (±6.5) for Sr and Ba, respectively (Figs. 5a,b). The results (i.e., differential slopes) show that the sensitivity of Ba partitioning between apatite and water as a function of the yield is greater than for Sr. Constant stirring of the solutions resulted in a shift of R% and $K_{a\text{-}w}^{Ba/Ca}$ values but they still lie on the regression line obtained from experiments performed without stirring (Fig. 5b). This confirms that before the steady-state was reached, the $K_{a\text{-}w}^{Sr/Ca}$ and $K_{a\text{-}w}^{Ba/Ca}$ values were controlled by the crystallography of the

Table 4. Influence of the starting pH value of the solution on R% and $K_{a\text{-}w}^{Ba/Ca}$ values after 24 hours and 48 hours of maturation. Each second line in italic indicates the respective SD values.

48 hours	pH_i = 10.8	pH_i = 9.8
$K_{a\text{-}w}^{Ba/Ca}$	0.161	0.172
	0.019	*0.014*
R (%)	52.8	48.2
	0.1	*0.1*
24 hours	**pH_i = 10.8**	**pH_i = 9.8**
$K_{a\text{-}w}^{Ba/Ca}$	0.235	0.247
	0.031	*0.044*
R (%)	54.2	49.2
	0.5	*0.8*

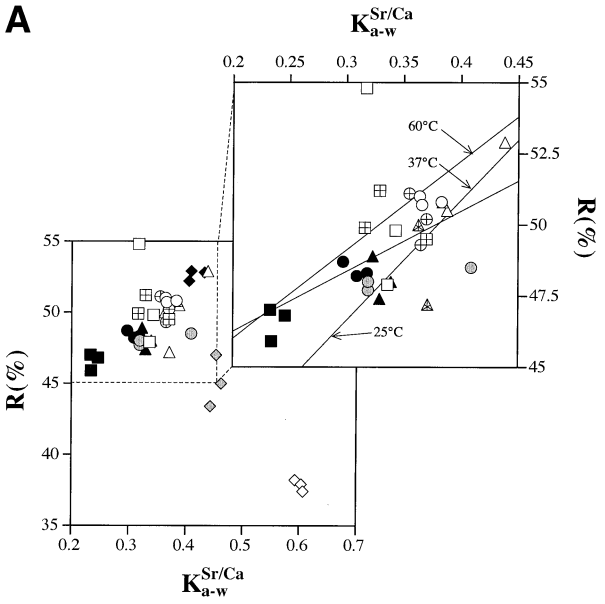

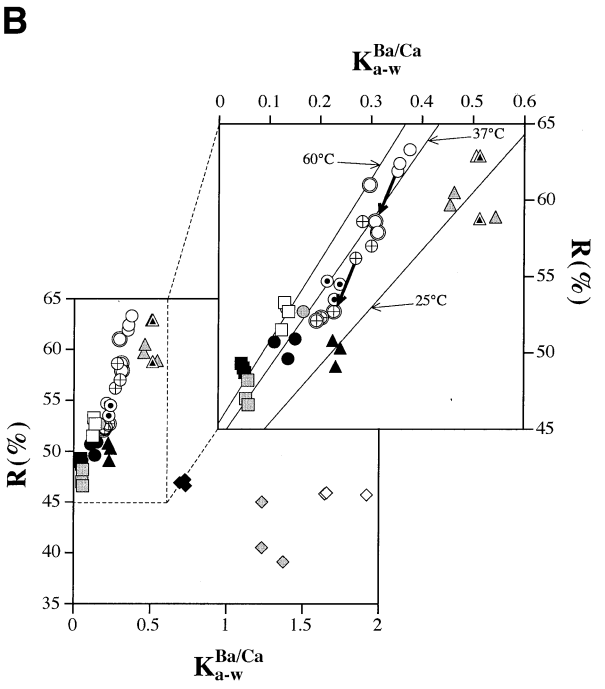

Fig. 5. (a) Relation between Sr partition coefficients ($K_{a\text{-}w}^{Sr/Ca}$) and reaction yields (R%). Diamonds, triangles, circles and squares are for 5°C, 25°C, 37°C, and 60°C, respectively. Open, crossed, gray filled, and black filled symbols are for 1 h, 6 h, 48 h, and 96 h of experiment, respectively. Coefficients a, b and r^2 of the linear regression R% = a. $K_{a\text{-}w}^{Sr/Ca}$ + b are 42.3 (±12.3), 33.9 (±4.6), and 0.66 at 25°C; 21.2 (±9.9), 42.0 (±3.5), and 0.32 at 37°C; 31.2 (±16.2), 39.8 (±5.0), and 0.34 at 60°C. (b) Relation between Ba partition coefficients ($K_{a\text{-}w}^{Ba/Ca}$) and reaction yields (R%). Same symbols as in (a). Doubled circles are for stirred phosphate solutions and the corresponding nonstirred samples are linked by an arrow. Surrounded filled triangles and circles are for 25°C/24 h and 37°C/24 h respectively. Coefficients a, b and r^2 of the regression line R% = a. $K_{a\text{-}w}^{Ba/Ca}$ + b are 37.9 (±5.3), 41.6 (±2.3), and 0.88 at 25°C; 48.2 (±4.0), 44.2 (±1.0), and 0.92 at 37°C; 53.7 (±10.9), 45.4 (±0.9), and 0.78 at 60°C.

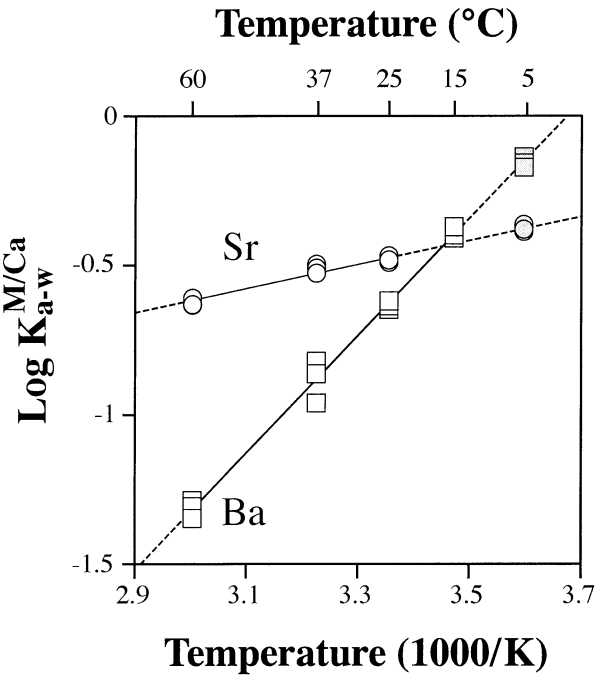

Fig. 6. Variations of Log($K_{a\text{-}w}^{M/Ca}$) as a function of the inverse of temperature. Straight lines are Log($K_{a\text{-}w}^{Sr/Ca}$) = 0.42 ± 0.04 (10^3 T^{-1}) − 1.87 ± 0.12 (r^2 = 0.94) and Log($K_{a\text{-}w}^{Ba/Ca}$) = 1.96 ± 0.06 (10^3 T^{-1}) − 7.19 ± 0.20 (r^2 = 0.99). Open and filled symbols are for HAP and ACP + DCPD respectively.

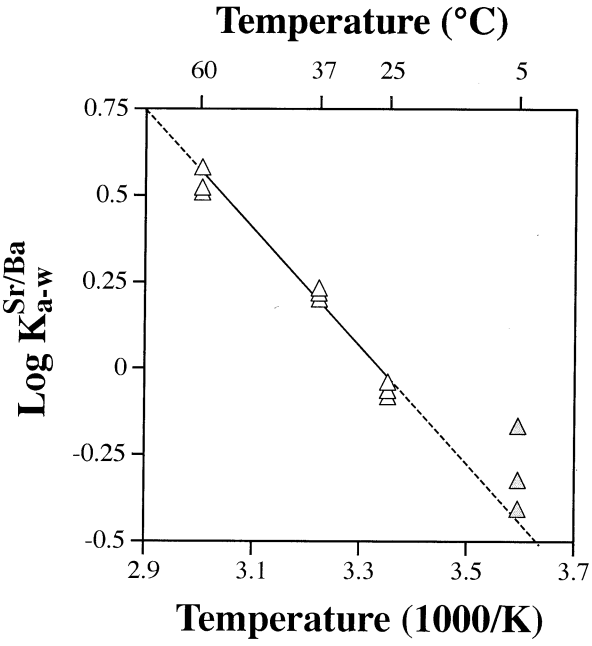

Fig. 7. Variations of Log($K_{a\text{-}w}^{Sr/Ba}$) as a function of the inverse of temperature. The straight line is Log($K_{a\text{-}w}^{Sr/Ba}$) = −0.75 ± 0.04 (10^3 T^{-1}) + 2.39 ± 0.14 (r^2 = 0.97). Open and filled symbols are for HAP and ACP + DCPD respectively.

Table 5. Sr and Ba concentrations in the PO_4^{3}-bearing liquid and solid phases, calculated Sr/Ba partition coefficients ($K_{a\text{-}w}^{Sr/Ba}$), and corresponding reaction yields (R%) of PO_4^{3-}-bearing precipitates. Each second line in italic indicates the respective SD values.

Temperature (°C)	Liquid phase			Solid phase				
	Sr (mmol/L)	Ba (mmol/L)	Sr/Ba	Sr (mmol/g)	Ba (mmol/g)	Sr/Ba	$K_{a\text{-}w}^{Sr/Ba}$	R (%)
60	0.36	0.47	0.492	0.42	0.15	2.794	3.621	43.7
	0.01	*0.02*	*0.004*	*0.03*	*0.01*	*0.162*	*0.213*	*0.2*
37	0.35	0.39	0.571	0.40	0.26	1.549	1.733	22.7
	0.00	*0.00*	*0.003*	*0.01*	*0.01*	*0.021*	*0.034*	*0.3*
25	0.40	0.38	0.662	0.36	0.39	0.915	0.882	45.6
	0.05	*0.05*	*0.000*	*0.01*	*0.00*	*0.013*	*0.012*	*0.7*
5	0.36	0.28	0.824	0.39	0.60	0.673	0.530	20.2
	0.00	*0.02*	*0.063*	*0.03*	*0.12*	*0.088*	*0.113*	*2.0*

solid phase which evolved most probably driven by a kinetic process of diffusion-controlled growth (Lasaga, 1998).

Results from the experiments performed with a starting pH of 9.8 are shown in Table 4. A comparison with the experiments carried out with a starting pH of 10.8 reveals that the initial pH condition only affects the yield of the reactions while the $K_{a\text{-}w}^{Ba/Ca}$ values are similar after 24 and 48 h of ageing.

3.5. The Sr/Ca, Ba/Ca, and Sr/Ba Thermometers

At steady-state conditions (i.e., after 96 h of ageing) and excluding the data obtained from ACP and DCPD mixtures, the strong temperature dependencies of $K_{a\text{-}w}^{Sr/Ca}$, $K_{a\text{-}w}^{Ba/Ca}$, and $K_{a\text{-}w}^{Sr/Ba}$ can be represented by the following linear equations (Figs. 6 and 7; Table 5) :

$$\mathrm{Log}(K_{a\text{-}w}^{Sr/Ca}) = 0.42 \pm 0.04\,(10^3 T^{-1}) - 1.87 \pm 0.12\ (r^2 = 0.94) \quad (2)$$

$$\mathrm{Log}(K_{a\text{-}w}^{Ba/Ca}) = 1.96 \pm 0.06\,(10^3 T^{-1}) - 7.19 \pm 0.20\ (r^2 = 0.99) \quad (3)$$

$$\mathrm{Log}(K_{a\text{-}w}^{Sr/Ba}) = -0.75 \pm 0.04\,(10^3 T^{-1}) + 2.39 \pm 0.14\ (r^2 = 0.97) \quad (4)$$

It is interesting to note that the sensitivities with respect to temperature of the Sr partition coefficients between apatite and water are of the same order of magnitude as for inorganic aragonite (ar) and water. From the data of Kinsman and Holland (1969), we derived a value of 0.20 ± 0.03 for the slope of the regression line between $K_{ar\text{-}w}^{Sr/Ca}$ and 10^3/T (K). This slope is comparable to the value of 0.42 ± 0.04 inferred from the present study for the apatite-water system.

Using a pH-stat system to maintain the ionic strength and the pH constant during the precipitation of HAP from a slightly supersaturated aqueous solution, Neuman et al. (1963) calculated a $K_{a\text{-}w}^{Sr/Ca}$ of 0.21 at 25°C. From the present study, where only steady-state conditions can be assessed, we derived a $K_{a\text{-}w}^{Sr/Ca}$ of 0.33 ± 0.01 at 25°C which is similar to the value reported by Neuman et al. (1963).

Only a few data are available so far for Sr and Ba concentrations in the phosphatic hard tissues of ectotherms organisms and associated water. However, the partition coefficients deduced from Eqns. 2 and 3 may be compared with those derived from experimental results (Wells et al., 2000) on fish scales (*Leiostomus xanthurus*). At temperatures between 20 and 25°C these authors measured $K_{a\text{-}w}^{Sr/Ca}$ and $K_{a\text{-}w}^{Ba/Ca}$ values of 0.16 ± 0.01 and 0.39 ± 0.01 respectively, which are of the same order of magnitude as our values of 0.33 ± 0.01 and 0.23 ± 0.01 at 25°C.

Ba/Ca and Sr/Ca ratios have been measured in fish teeth sampled across the K/T boundary recorded in the phosphorite deposits of Morocco. The trend defined by the Ba/Ca ratios through time, mimics the evolution of oxygen isotope compositions that were measured by Lécuyer et al. (1993) on the same sample collection (Fig. 8). However, no correlation is observed when using the Sr/Ca ratios of fossil fish teeth (Table 6), most likely indicating a postdepositional perturbation of their Sr contents. Paleo-temperatures based on the Ba/Ca ratios were calculated by considering a hypothetical seawater Ba/Ca ratio of 10^{-3}. For further interpretation, this calculation requires an intercalibration with the oxygen isotope thermometer on living fishes. Considering that Ba/Ca ratios of fish teeth are not sensitive to changes in the volume of continental ice, the covarying trends defined by the two proxies confirm that the evolution of the oxygen isotope compositions of fish teeth mainly results from variations in the sea surface temperatures. The combination of oxygen isotope compositions with trace

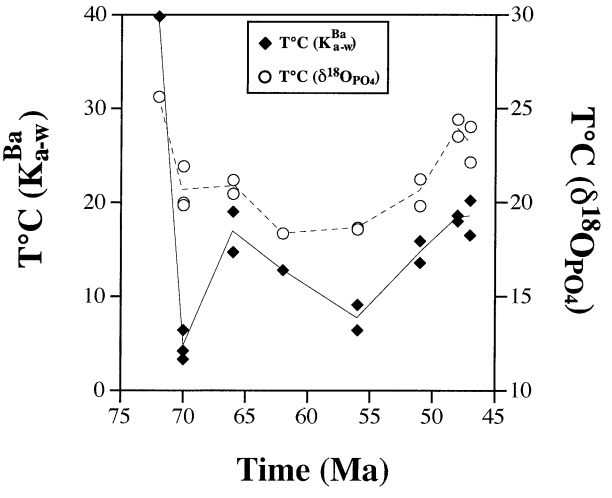

Fig. 8. Evolution of temperatures derived from $\delta^{18}O(PO_4)$ and Ba/Ca ratios from fish teeth sampled across the K/T boundary of Morocco (see Lécuyer et al., 1993).

Table 6. Taxonomy, location, age, Sr, Ba concentrations, $\delta^{18}O_{PO4}$ values of fossil fish teeth recovered from the K/T boundary and Ba/Ca-derived and $\delta^{18}O_{PO4}$-derived paleotemperatures. The $\delta^{18}O_{PO4}$-derived paleotemperatures were calculated according to Kolodny et al. (1983). The Ca content was assumed to be 40% (wgt %). The Sr-derived temperatures range from 45 to 165°C with a seawater Sr/Ca ratio of 0.02. All these samples came from Morocco and were described in Lécuyer et al. (1993).

Taxonomy	Location	Age (Ma)	Sr (μg/g)	Ba (μg/g)	$\delta^{18}O_{PO4}$ (‰ SMOW)	T°C (Ba/Ca)	T°C ($\delta^{18}O_{PO4}$)
Cretolamna sp.	Oued Erguita	72	2000	38.7	18.9	44.0	25.6
Squalicorax	Ganntour	70	1638	240	20.3	8.1	20.0
Squalicorax pristodontus	Ganntour	70	2187	254	20.3	7.1	19.9
Hypsobatis	Ganntour	70	1368	211	19.8	10.3	21.9
Cretolamna biauriculata	Sidi Daoui	66	1510	132	20.0	18.9	21.2
Rhombodus binkhorski	Sidi Daoui	66	1226	105	20.1	23.3	20.5
Dasyatis hexagonalis	Sidi Daoui	62	1350	147	20.6	16.9	18.3
Striatolamia sp.	Ouled Abdoun	56	1367	211	20.6	10.3	18.6
Myliobatis sp.	Ouled Abdoun	56	1354	181	20.6	13.1	18.6
Striatolamia sp.	Ouled Abdoun	51	1217	141	20.0	17.7	21.2
Myliobatis sp.	Ouled Abdoun	51	996	124	20.3	20.1	19.8
Striatolamia sp.	Ouled Abdoun	48	1168	107	19.4	22.9	23.5
Myliobatis sp.	Ouled Abdoun	48	1098	111	19.2	22.2	24.4
Striatolamia sp.	Ouled Abdoun	47	1204	99	19.8	24.5	22.1
Myliobatis sp.	Ouled Abdoun	47	1167	120	19.3	20.7	24.0

element contents of marine biogenic apatites appears to be a potentially powerful biogeochemical tool for deciphering both ice volume and temperature variations in the marine environment. We emphasize, however, that a detailed investigation of diagenetic alteration is a prerequisite before using the trace element content of biogenic apatites as a paleothermometer of aquatic environments. In addition, more experimental studies will be necessary to investigate the possible influence of the so-called vital effects on the Sr and Ba partition coefficients between biogenic apatite and the aqueous environment.

4. CONCLUSIONS

Experimental determinations of Sr and Ba partition coefficient between inorganic hydroxyapatite and water were determined at temperatures ranging from 5°C to 60°C. They displayed a high sensitivity relative to temperature, providing a new potential paleothermometer for aquatic environments. Their combination with paleothermometers based on the fractionation of oxygen isotopes applied to biogenic apatites should help to evaluate salinity variations at the scale of a water mass or at the scale of the global ocean in response to glacial events. However, a safe application of this method to biogenic apatites will require an investigation of the influence of biologic activity on trace element fractionation (i.e., so-called vital effects) and to evaluate if potential offsets relative to the inorganic system are species-dependent. Diagenetic alteration of apatites is also expected to modify their original trace element ratios and therefore should be diagnosed before any interpretation of paleotemperatures for a given water composition.

Acknowledgments—The authors thank G. Gruau, B. Reynard, E. Rose-Koga, P.P. Zuddas and two anonymous reviewers for their very helpful comments. The scientific and editorial comments of A. Mucci greatly improved the quality of this manuscript. We also thank M. Bouhnik-Le Coz and C. Douchet for the ICP-MS and ICP-AES measurements and Ruben Vera for XRD measurements. This work was funded by the French CNRS program ECLIPSE.

Associate editor: A. Mucci

REFERENCES

Abbona F. and Franchini-Angela M. (1990) Crystallization of calcium and magnesium phosphates from solutions of low concentration. *J. Crystal Growth* **104,** 661–671.

Blake R. E., O'Neil J. R., and Garcia G. A. (1998) Effects of microbial activity on the $\delta^{18}O$ of dissolved inorganic phosphate and textural features of synthetic apatites. *Am. Mineral.* **83,** 1516–1531.

Boskey A. L. and Posner A. S. (1976) Formation of hydroxyapatite at low supersaturation. *J. Chem. Phys.* **80,** 40–45.

Brecevic L. and Furedi-Milhofer H. (1972) Precipitation of calcium phosphates from electrolyte solutions. II. The formation and transformation of the precipitates. *Calcif. Tiss. Res.* **10,** 82–90.

Broecker W. S. and Peng T. H. (1982) Tracers in the Sea. Eldigio Press.

Christoffersen M. R., Christoffersen J., and Kibalczic W. (1990) Apparent solubilities of two amorphous calcium phosphates and of octacalcium phosphate in the temperature range 30–42°C. *J. Crystal Growth* **106,** 349–354.

Eanes E. D., Gillessen I. H., and Posner A. S. (1965) Intermediate states in the precipitation of hydroxyapatite. *Nature* **208,** 365–367.

Furedi-Milhofer H., Purgaric B., Brecevic L., and Pavkovic N. (1971) Precipitation of calcium phosphates from electrolyte solutions. I. A study of the precipitates in the physiological region. *Calcif. Tiss. Res.* **8,** 142–153.

Henderson L. M. and Kracek F. C. (1927) The fractional precipitation of barium and radium chromates. J. Am. Chem. Soc. **49,** 739–749.

JCPDS 1 (Joint Committee on Powder Diffraction Standards–International Center for Diffraction Data). (1990) File 09-0432. JCPDS.

JCPDS 2 (Joint Committee on Powder Diffraction Standards–International Center for Diffraction Data). (1990) File 11-0293. JCPDS.

Kaim W. and Schewderski B. (1994) Bioinorganic Chemistry: Inorganic Elements in the Chemistry of Life—An Introduction and Guide. Wiley.

Kinsman J. J. and Holland H. D. (1969) The coprecipitation of cations CaCO3-IV. The coprecipitation of Sr^{2+} with aragonite between 16° and 96°. *Geochim. Cosmochim. Acta* **33,** 1–18.

Kolodny Y., Luz B., and Navon O. (1983) Oxygen isotope variations in phosphate of biogenic apatites, I. Fish bone apatite-rechecking the rules of the game. *Earth Planet. Sci. Lett.* **64,** 398–404.

Lasaga A. (1998) Kinetic Theory in the Earth Sciences. Princeton University Press.

Lécuyer C., Grandjean P., O'Neil J. R., Cappetta H., and Martineau F. (1993) Thermal excursion in the ocean at the Cretaceous-Tertiary boundary (Northern Morocco): $\delta^{18}O$ record of phosphatic fish debris. *Palaeogeogr. Palaeoclimatol. Palaeoecol.* **105,** 235–243.

Lécuyer C., Grandjean P., Paris F., Robardet M., and Robineau F. (1996) Deciphering "temperature" and "salinity" from biogenic

phosphates: The $\delta^{18}O$ of coexisting fishes and mammals of the Middle Miocene sea of western France. *Palaeogeogr. Palaeoclimatol. Palaeoecol.* **126,** 61–74.

Lécuyer C., Picard S., Garcia J. P., Sheppard S. M. F., Grandjean P., and Dromart G. (in press) Thermal evolution of Tethyan surface waters during the Middle-Late Jurassic: Evidence from $\delta^{18}O$ values of marine fish teeth. *Paleoceanography*.

LeGeros R. Z. and LeGeros J. P. (1984) Phosphate minerals in human tissues. In *Phosphate Minerals* (eds. J. O. Nriagu and P. B. Moore), pp. 351–385. Springer-Verlag.

Longinelli A. and Nuti S. (1973) Oxygen isotope measurements of phosphate from teeth and bones. *Earth Planet. Sci. Lett.* **20,** 337–340.

McCulloch M. T., Gagagn M. K., Mortimer G. E., Chivas A. R., and Isdale P. J. (1994) A high resolution Sr/Ca and $\delta^{18}O$ coral record from the Great Barrier Reef, Australia, and the 1982–1983 El Niño. *Geochim. Cosmochim. Acta.* **58,** 2747–2754.

McIntire W. L. (1963) Trace element partition coefficients-a review of theory and applications to geology. *Geochim. Cosmochim. Acta* **27,** 1209–1264.

Monnin C., Jeandel C., Cattaldo T., and Dehairs F. (1999) The marine barite saturation state of the world's oceans. *Mar. Chem.* **65,** 253–261.

Nancollas G. H. (1984) The nucleation and growth of phosphate minerals. In *Phosphate Minerals* (eds. J. O. Nriagu and P. B. Moore), pp. 137–154. Springer-Verlag.

Neuman W. F., Bjornerstedt R., and Mulryan B. J. (1963) Synthetic hydroxyapatite crystals. II Ageing and strontium incorporation. *Arch. Biochem. Biophys.* **101,** 215–224.

Paytan A. and Kastner M. (1996) Benthic Ba fluxes in the central Equatorial Pacific, implications for the oceanic Ba cycle. *Earth Planet. Sci. Lett.* **142,** 439–450.

Pucéat E., Lécuyer C., Sheppard S. M. F., Dromart G., Reboulet S., and Grandjean P. (2003) Thermal evolution of Cretaceous Tethyan marine waters inferred from oxygen isotope composition of fish tooth enamels. *Paleoceanography* **18**.

Schenau S. J., Slomp C. P., and De Lange G. J. (2000) Phosphogenesis and active phosphorite formation in sediments from the Arabian Sea oxygen minimum zone. *Mar. Geol* **169,** 1–20.

Van Cappellen P. and Berner R. A. (1991) Fluorapatite crystal growth from artificial seawater. *Geochim. Cosmochim. Acta* **55,** 1219–1234.

Wells B. K., Bath G. E., Thorrold S. R., and Jones C. M. (2000) Incorporation of strontium, cadmium and barium in juvenile spot (*Leiostomus xanthurus*) scales reflects water chemistry. *Can. J. Aquat. Sci.* **57,** 2122–2129.

Wenzel B., Lécuyer C., and Joachimski. (2000) Comparing oxygen isotope records of Silurian calcite and phopshate-$\delta^{18}O$ compositions of brachiopods and conodonts. Geochim. Cosmochim. Acta **64** 1859–1872.

Young R. A. and Holcomb D. W. (1982) Variability of hydroxyapatite preparations. *Calcif. Tissue Int.* **34,** 17–32.